Supporting Information

Highly Fluorescent Chameleon Nanoparticles and Polymer Films: Multi-Component Organic Systems that Combine FRET and Photochromic Switching

Sanghoon Kim, Seong-Jun Yoon, Soo Young Park*

Complete reference

[15] M. J. Frisch, G. W. Trucks, H. B. Schlegel, G. E. Scuseria, M. A. Robb, J. R. Cheeseman, G. Scalmani, V. Barone, B. Mennucci, G. A. Petersson, H. Nakatsuji, M. Caricato, X. Li, H. P. Hratchian, A. F. Izmaylov, J. Bloino, G. Zheng, J. L. Sonnenberg, M. Hada, M. Ehara, K. Toyota, R. Fukuda, J. Hasegawa, M. Ishida, T. Nakajima, Y. Honda, O. Kitao, H. Nakai, T. Vreven, J. A. Montgomery, Jr., J. E. Peralta, F. Ogliaro, M. Bearpark, J. J. Heyd, E. Brothers, K. N. Kudin, V. N. Staroverov, R. Kobayashi, J. Normand, K. Raghavachari, A. Rendell, J. C. Burant, S. S. Iyengar, J. Tomasi, M. Cossi, N. Rega, J. M. Millam, M. Klene, J. E. Knox, J. B. Cross, V. Bakken, C. Adamo, J. Jaramillo, R. Gomperts, R. E. Stratmann, O. Yazyev, A. J. Austin, R. Cammi, C. Pomelli, J. W. Ochterski, R. L. Martin, K. Morokuma, V. G. Zakrzewski, G. A. Voth, P. Salvador, J. J. Dannenberg, S. Dapprich, A. D. Daniels, O. Farkas, J. B. Foresman, J. V. Ortiz, J. Cioslowski, and D. J. Fox, Gaussian 09, Revision A.02, Gaussian, Inc., Wallingford CT, **2009**.

General method and materials

Materials. All commercially available reagents and solvents were purchased from Sigma-Aldrich, Alfa Aesar, TCI, and Junsei and used without further purification, unless otherwise stated.

Instruments. *Nuclear Magnetic Resonance (NMR) Spectroscopy.* All ^{1}H NMR spectra were recorded with a Bruker Avance-300 (300 MHz) in $CDCl_3$ solutions. ^{13}C NMR spectra were recorded with a Bruker Avance-500 (500 MHz) in $CDCl_3$ solutions.

Elemental Analysis. Elemental analysis was carried out using a CE instruments EA1110 elemental analyzer. Mass Spectra were measured with a JEOL JMS AX505WA mass spectrometer.

UV-Visible Absorption Spectroscopy. UV-visible absorption spectra were recorded on a Shimadzu UV-1650PC UV-visible spectrophotometer using samples in solution or samples coated on quartz film.

Fluorescence Spectroscopy. Fluorescence spectra were recorded on a Varian Cary Eclipse fluorescence spectrometer with samples in solution or samples coated on quartz film.

Spin-Coating. Spin-coating was carried out with a Midas SPIN-1200D spin process controller.

Visible Light Irradiation. Visible light irradiation was carried out with Oriel instruments 66028 xenon arc lamp, Oriel instruments 68811 arc lamp power supply, Oriel instruments 77250 monochrometer, and Newport FS-C color filter (> 550 nm).

UV Light Irradiation. UV light irradiation was carried out with a Vilber Lourmat VL-4.LC hand-held lamp (365 nm). The fluorescence images were obtained with a digital camera (Canon PowerShot G6 and S45) under illumination at 365 nm with hand-held lamp.

Time-Resolved Fluorescence Spectroscopy. Time-resolved fluorescence measurement was carried out with nanoparticles' suspension in quartz cell and spin-coated quartz film by PicoQuant DLP 800-D pulsed diode laser, PicoQuant PicoHarp 300 TCSPC module and picoseconds event timer, and PicoQuant FluoTime 200 time-resolved spectrometer.

Optical Microscopic Observation. Optical microscopic observation of the films was carried out with a Leica Mikroskopie & Systeme GmbH Wetzier.

Field Emission Scanning Electron Microscopy (FE-SEM). FE-SEM images were acquired on a Carl Zeiss, SUPRA 55VP.

Discussion. *Quantum Chemical Calculation.* DFT optimization calculations and time-dependent DFT (TD-DFT) excitation energy calculations were performed with the Gaussian 09 software. The ground-state geometry was fully optimized using the B3LYP functional and 6-31g (d,p) basis set.

FRET Efficiency Calculation. FRET efficiency was calculated experimentally with commonly defined as

$$E = 1 - \frac{F_{DA}}{F_D}$$

where F_{DA} and F_D is the maximum fluorescence intensity of the donor (CN-MBE in the two components system) in the presence of the acceptor (TPA-2CNMBE in the two components system) and absence of acceptor, respectively.

Experimental Section. *PLQY measurement.* The relative fluorescence quantum yield was measured using 9,10-diphenylanthracence (DPA) in benzene as a standard reference (1×10^{-4} mol L^{-1}, $\Phi_F = 0.83$).

UV/visible Light Irradiation. UV light irradiation was carried out with the hand-held lamp (365 nm, 1.2 mW cm^{-2}) from a distance of 5 cm. Visible light irradiation (> 550 nm) was carried out with the xenon lamp (1.5 mW cm^{-2}) and the color filter (> 550 nm) from a distance of 10 cm. Visible light irradiation (420 nm) for non-destructive read-out test was carried out with the xenon lamp (1.5 mW cm^{-2}) and the monochrometer from a distance of 10 cm. Film patterning via UV/visible light was carried out with UV and visible light sources and a pattern-printed transparency film.

Solvent-Vapor Annealing (SVA) Treatment. For SVA treatment, turned upside down spin-coated film placed at the mouth of a 20 ml or 8 ml vial containing 3ml dichloromethane (DCM) for about 10 minutes at room temperature.

Synthesis

Scheme S1. The synthetic route used to obtain compound TPS-CNMBE is shown below.

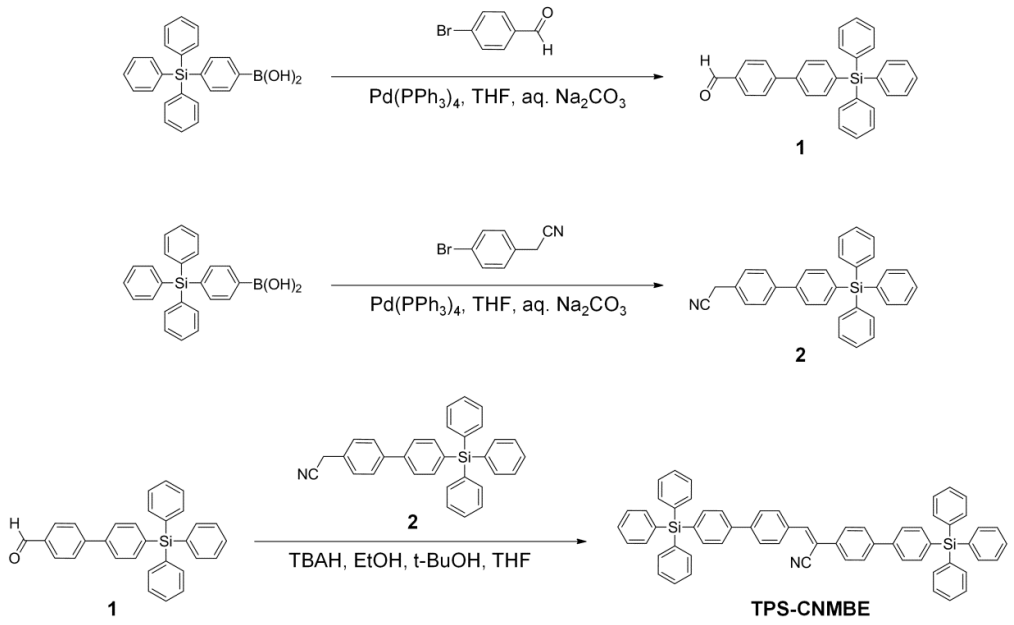

4'-(triphenylsilyl)-[1,1'-biphenyl]-4-carbaldehyde (1): (4-(triphenylsilyl)phenyl)boronic acid (1 g, 2.6294 mmol), 4-bromobenzaldehyde (0.4423 g, 2.3906 mmol), and tetrakis(triphenyl phosphine) palladium (0) (0.0331 g, 0.0287 mmol) were dissolved in 50 ml of tetrahydrofuran (THF) and 25 ml of 2N Na_2CO_3 aqueous solution and refluxed at 80 ℃ for 14 hours. After cooling to room temperature, the resulting mixture was poured into distilled water and the organic layer was extracted with ethyl acetate and dried with anhydrous magnesium sulfate. The resulting mixture was purified by the column chromatography (silica gel; ethyl acetate : *n*-hexane = 1 : 9) to give white power product (0.8291 g, 79 % yield); ^{1}H NMR ($CDCl_3$, 300 MHz): δ (ppm) 10.06 (s, 1H, CHO), 7.97 (d, 2H, 1-benzene), 7.79 (d, 2H, 1-benzene), 7.70 (m, 12H, 1-benzene), 7.48 (m, 9H, 1-benzene).

2-(4'-(triphenylsilyl)-[1,1'-biphenyl]-4-yl)acetonitrile (2): (4-(triphenylsilyl)phenyl)boronic acid (1 g, 2.6294 mmol), 2-(4-bromophenyl)acetonitrile (0.4686 g, 2.3903 mmol), and tetrakis(triphenyl phosphine) palladium (0) (0.0331 g, 0.0287 mmol) were dissolved in 30 ml of tetrahydrofuran (THF) and 15 ml of 2N Na_2CO_3 aqueous solution and refluxed at 80 ℃ for 14 hours. After cooling to room temperature, the resulting mixture was poured into distilled water and the organic layer was extracted with ethyl acetate and dried with anhydrous magnesium sulfate. The resulting mixture was purified by the column chromatography (silica gel; ethyl acetate : *n*-hexane = 1 : 5) to give pale yellow power product (0.7017 g, 65 % yield); ^{1}H NMR ($CDCl_3$, 300 MHz): δ (ppm) 7.67 (m, 12H, 1-benzene), 7.48 (m, 11H, 1-benzene), 7.48 (m, 11H, 1-benzene), 3.79 (s, 2H, methylene).

(Z)-2,3-bis(4'-(triphenylsilyl)-[1,1'-biphenyl]-4-yl)acrylonitrile (3, TPS-CNMBE): The mixture of **1** (0.7017 g, 1.5537 mmol) and **2** (0.6846 g, 1.5537 mmol) in *tert*-butyl alcohol (60 ml) and THF (13 ml) was stirred at 50 ℃ for 1 hour. Tetrabutylammonium hydroxide (TBAH) (1 M solution in methanol) (0.1553 ml) and ethanol (1.5 ml) was slowly dropped

into the mixture and stirred for 1 hour. The greenish yellow precipitate was collected by filtration and washed with methanol. Purification was done by flash column chromatography (silica gel, DCM) and reprecipitation with DCM and methanol gave pale greenish yellow powder (1.0828 g, 80 % yield); ^{1}H NMR ($CDCl_3$, 300 MHz): δ (ppm) 8.02 (d, 2H, 1-benzene), 7.80 (m, 45H, 1-benzene; vinyl). ^{13}C NMR ($CDCl_3$, 500 MHz): δ (ppm) 76.97, 77.23, 77.48, 111.27, 118.29, 126.65, 126.69, 127.80, 127.95, 128.18, 129.93, 130.14, 133.16, 133.91, 134.19, 134.44, 136.64, 137.26, 141.14, 141.18, 141.55, 141.99, 143.20. MS (FAB) (calcd for $C_{63}H_{47}NSi_2$, 874.2; found, 874) m/z: 874, 873, 796, 613, 460, 391, 341, 307, 259, 219, 154, 136, 55, 43. Anal. Calcd. for $C_{63}H_{47}NSi_2$: C, 86.55; H, 5.42; N, 1.60; Si, 6.43. Found: C, 86.39; H, 5.48; N, 1.62.

Scheme S2. The synthetic route used to obtain compound TPA-2CNMBE is shown below.

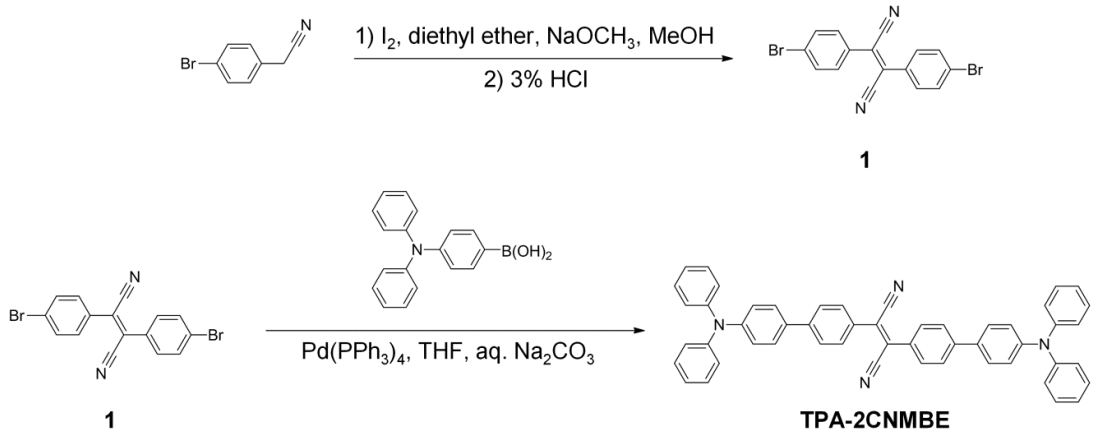

2,3-bis(4-bromophenyl)fumaronitrile (1): 2-(4-bromophenyl)acetonitrile (5 g, 25.505 mmol) and iodine (6.5734g, 25.505 mmol) were dissolved in dry diethyl ether (100 ml). Sodium methoxide (2.8933 g, 5.356 mmol) solution in methanol (8.680 g, 14.613 ml) was added slowly (over a period of 30 min) into the reaction solution at a dry-ice temperature under a argon atmosphere. The reaction solution was allowed to warm up by replacing the dry-ice bath with an ice–water bath before the temperature rose above 0 ℃. The reaction solution was further stirred for another 3–4 hours and then the reaction was quenched with 5 % hydrochloric acid. The reaction solution was further stirred for 12 hours. The resulting solution was filtered to isolate the solid, which was rinsed with cold methanol and water solution. The resulting mixture was dried. (3.1143 g, 63 % yield); ^{1}H NMR ($CDCl_3$, 300 MHz): δ (ppm) 7.73 (m, 8H, 1-benzene).

2,3-bis(4'-(diphenylamino)-[1,1'-biphenyl]-4-yl)fumaronitrile (2, TPA-2CNMBE): The compound **1** (0.5 g, 1.289 mmol), (4-(diphenylamino)phenyl)boronic acid (1.1940 g, 4.1295 mmol), and tetrakis(triphenyl phosphine) palladium (0) (0.0360 g, 0.0310 mmol) were dissolved in 15 ml of tetrahydrofuran (THF) and 5 ml of 2N Na_2CO_3 aqueous solution and stirred at 175 ℃ for 90 minutes in micro-wave reactor. After cooling to room temperature, the resulting mixture was poured into distilled water and the organic layer was extracted with ethyl acetate and dried with anhydrous magnesium sulfate. The resulting mixture was purified by the column chromatography (silica gel; DCM : *n*-hexane = 1 : 1). The resulting powder was purified by the reprecipitation in methanol to give red power product (0.46 g, 49.5 % yield).; ^{1}H NMR ($CDCl_3$, 300 MHz): δ (ppm) 7.94 (d, 4H, CHO), 7.74 (d, 4H, 1-benzene) , 7.54 (d, 4H, 1-benzene), 7.32 (t, 8H, 1-benzene), 7.17 (d, 12H, 1-benzene), 7.10 (t, 4H, 1-benzene). ^{13}C NMR ($CDCl_3$, 500 MHz): δ (ppm) 76.97, 77.23, 77.48, 117.28, 123.41, 123.66, 124.22, 125.10, 127.20, 127.31, 128.04, 128.10, 129.43, 129.56, 129.62, 130.56, 132.85, 144.14, 147.60, 148.56. MS (FAB) (calcd for $C_{52}H_{36}N_4$, 716.9; found, 716) m/z: 716, 613, 460, 443, 391, 341, 307, 289, 237, 219, 154, 136, 107, 89, 55, 43, 27. Anal. Calcd. for $C_{52}H_{36}N_4$: C, 87.12; H, 5.06; N, 7.82. Found: C, 87.05; H, 5.04; N, 7.84.

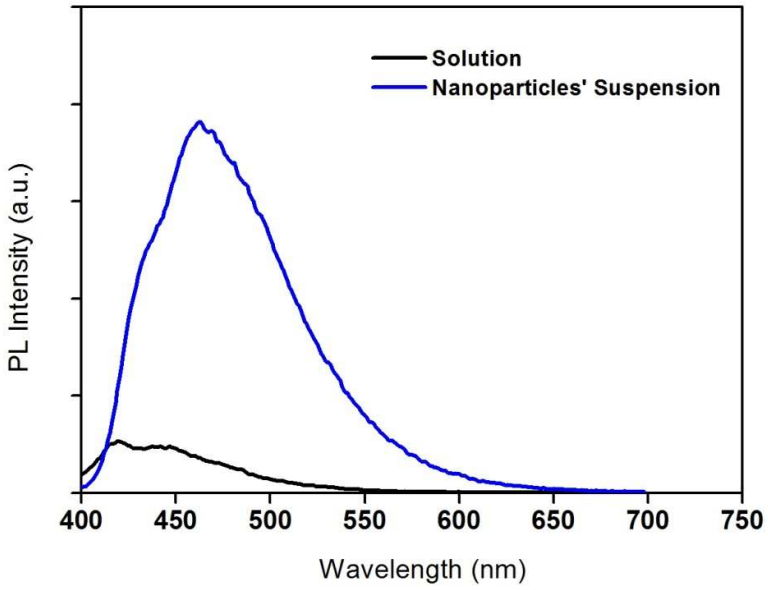

Figure S1. Fluorescence spectra of the TPS-CNMBE solution in THF (2×10^{-5} M) and the nanoparticles' suspension in THF/water mixture (2×10^{-5} M).

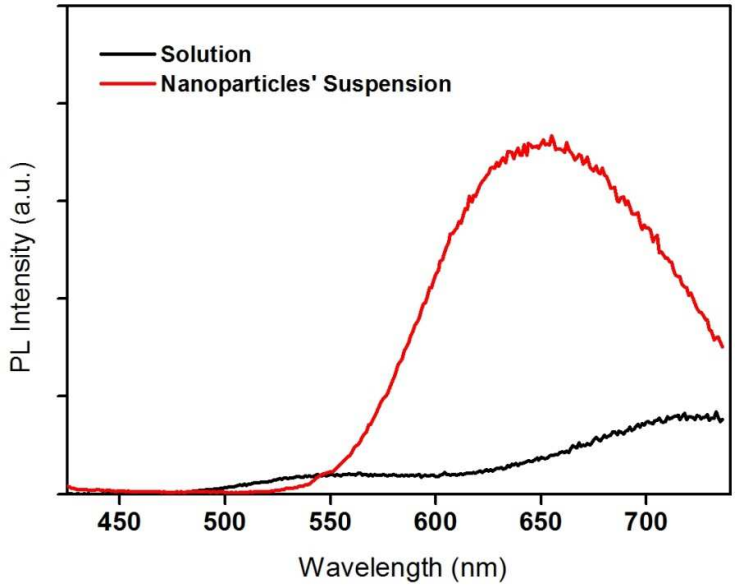

Figure S2. Fluorescence spectra of the TPA-2CNMBE solution in THF (2×10^{-5} M) and the nanoparticles' suspension in THF/water mixture (2×10^{-5} M).

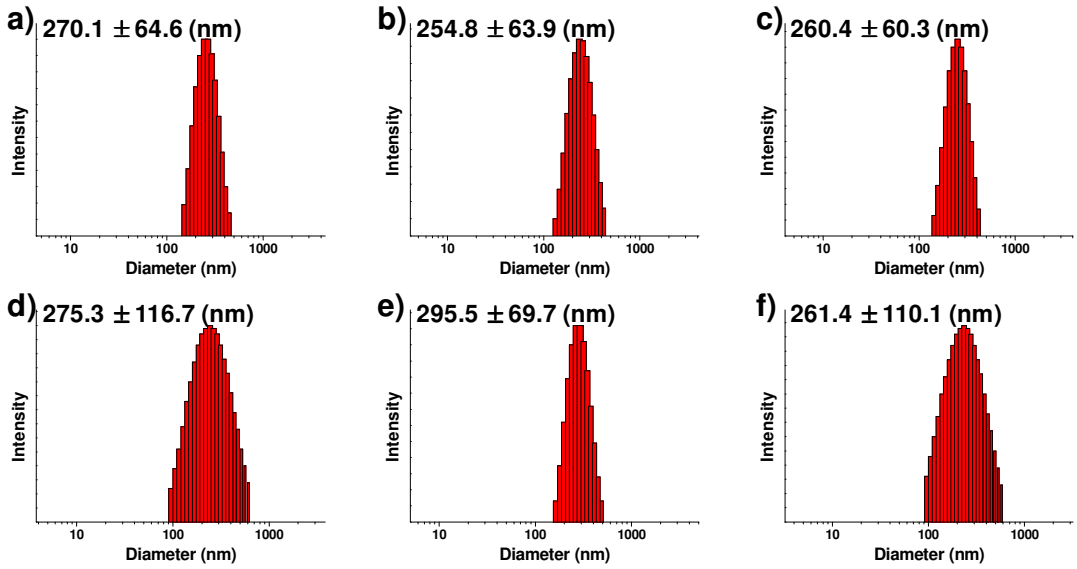

Figure S3. Size distribution and average size of nanoparticles suspensions in THF/water mixture (2×10^{-5} M): a) CN-MBE, b) CN-MBE/TPA-2CNMBE with 1 mol% of TPA-2CNMBE, c) CN-MBE/TPA-2CNMBE with 5 mol% of TPA-2CNMBE, d) CN-MBE/TPA-2CNMBE with 10 mol% of TPA-2CNMBE, e) TPA-2CNMBE, f) CN-MBE/TPA-2CNMBE/BP-BTE.

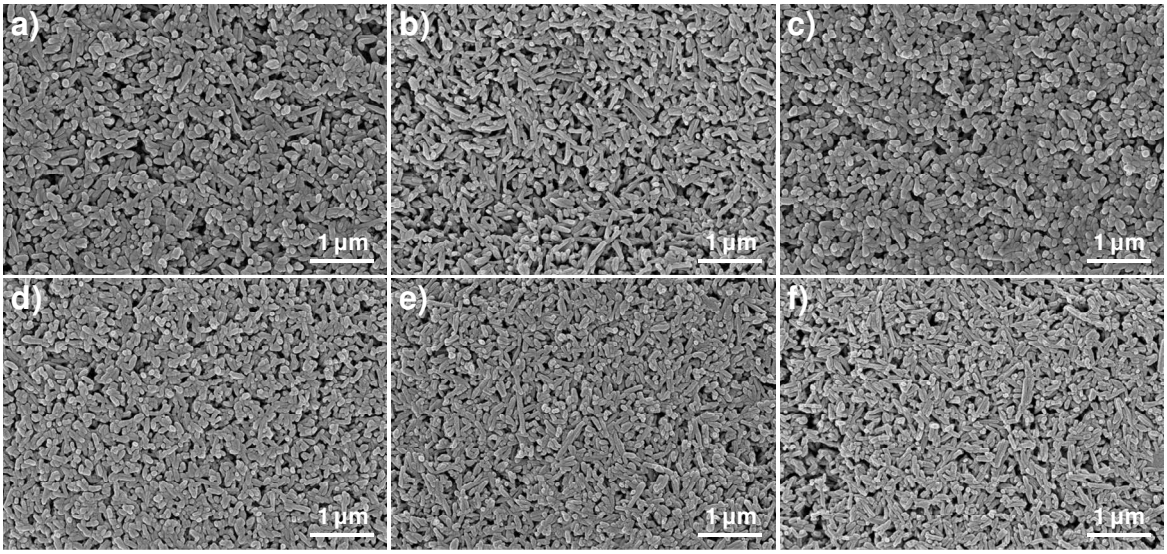

Figure S4. FE-SEM images of nanoparticles suspensions in THF/water mixture (2×10^{-5} M): a) CN-MBE, b) CN-MBE/TPA-2CNMBE with 1 mol% of TPA-2CNMBE, c) CN-MBE/TPA-2CNMBE with 5 mol% of TPA-2CNMBE, d) CN-MBE/TPA-2CNMBE with 10 mol% of TPA-2CNMBE, e) TPA-2CNMBE, f) CN-MBE/TPA-2CNMBE/BP-BTE.

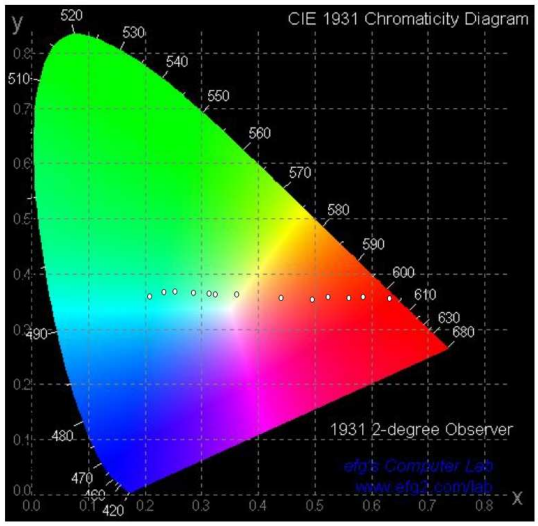

Figure S5. CIE 1931 chromaticity diagram with the fluorescence color of the CN-MBE/TPA-2CNMBE nanoparticles' suspensions with various TPA-2CNMBE molar ratios; 0, 0.1, 0.2, 0.5, 0.8, 1, 2, 5, 10, 20, 30, 50, 100 mol% of TPA-2CNMBE with respect to CN-MBE, respectively (points from left to right in the diagram; λ_{ex} = 400 nm).

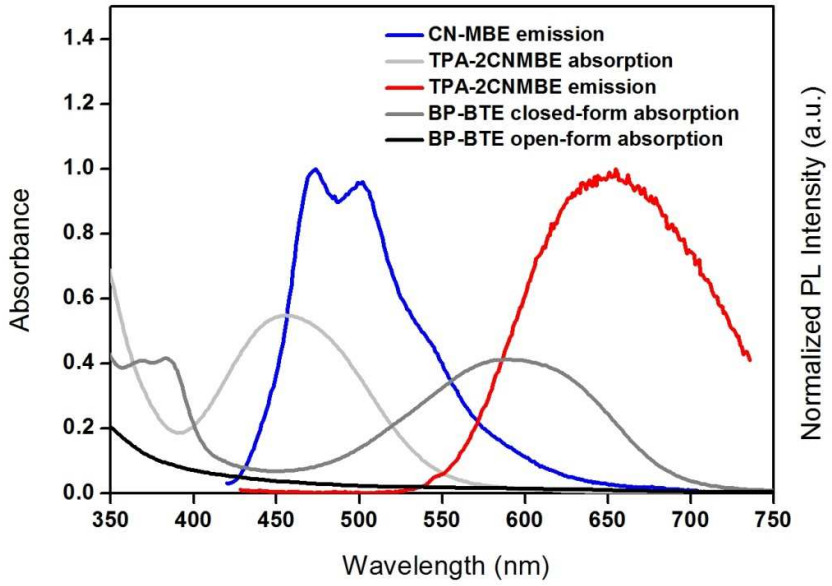

Figure S6. UV-visible absorption spectra of TPA-2CNMBE (light gray line), closed-form BP-BTE (gray line), open-form BP-BTE (black line) and fluorescence spectra of CN-MBE (blue line) and TPA-2CNMBE (red line). All sample are the nanoparticles' suspensions in THF/water mixture (2×10^{-5} M).

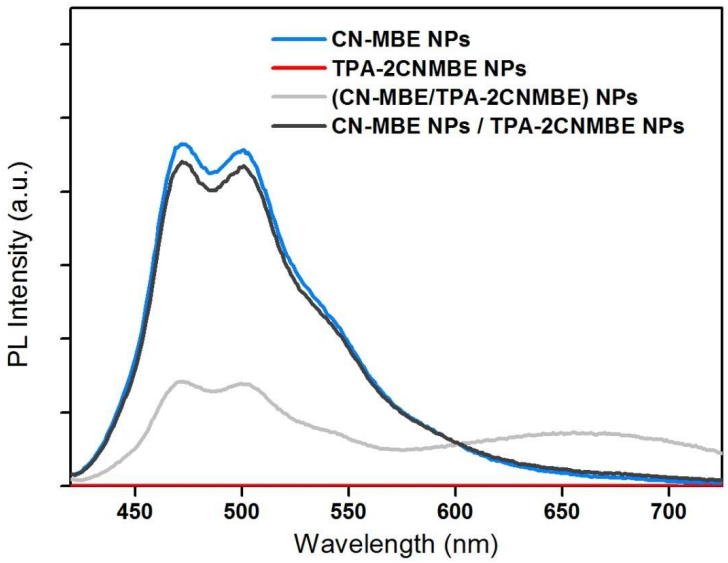

Figure S7. Fluorescence spectra of CN-MBE nanoparticles' suspension (1.98×10^{-5} M; sky blue line), TPA-2CNMBE nanoparticle's suspension (2×10^{-7} M; red line), CN-MBE/TPA-2CNMBE nanoparticles' suspension exhibiting intra-particle FRET (total concentration = 2×10^{-5} M, 1 mol% of TPA-2CNMBE; light gray line), TPA-2CNMBE nanoparticles and CN-MBE nanoparticles dispersed suspension exhibiting inter-particle FRET (total concentration = 2×10^{-5} M, 1 mol % of TPA-2CNMBE; dark gray line).

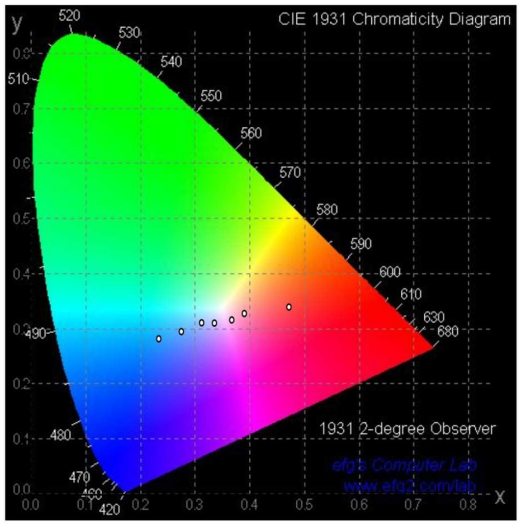

Figure S8. CIE 1931 chromaticity diagram with the fluorescence color (λ_{ex} = 400 nm) of the CN-MBE/TPA-2CNMBE/BP-BTE nanoparticles' suspensions with various UV light irradiation time (365 nm); The UV irradiation time was varied 0, 1, 3, 5, 7, 10, 15 seconds, respectively (points from right to left in the diagram).

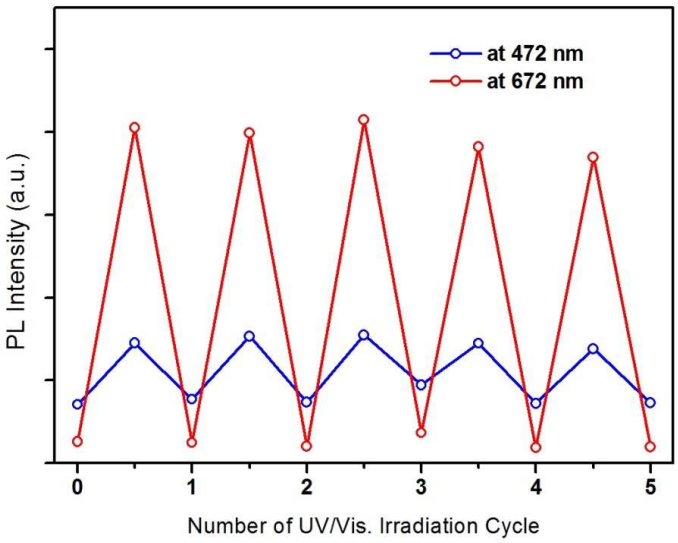

Figure S9. Reversible fluorescence color modulation of CN-MBE/TPA-2CNMBE/BP-BTE nanoparticles' suspension (λ_{ex} = 400 nm) driven by alternating UV and visible light irradiations ($\lambda_{monitor}$ = 472 nm for blue points, $\lambda_{monitor}$ = 672 nm for red points).

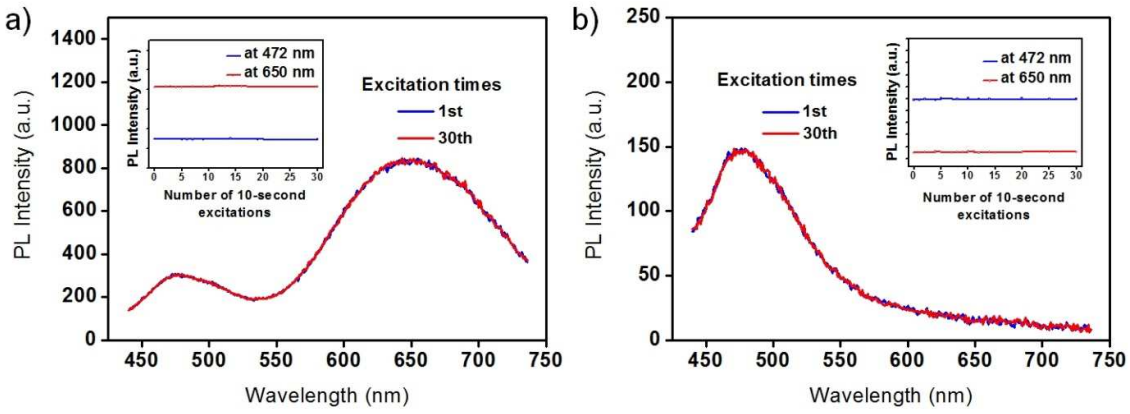

Figure S10. a,b) Fluorescence spectra (λ_{ex} = 420 nm) showing the non-destructive readout capability of CN-MBE/TPA-2CNMBE/BP-BTE nanoparticles' suspension in open-form sate of BP-BTE (a) and in closed-form state of BP-BTE (b); each inset shows the fluorescence spectra intensities at 472 nm (blue line) and 650 nm (red line) of the nanoparticles' suspension.

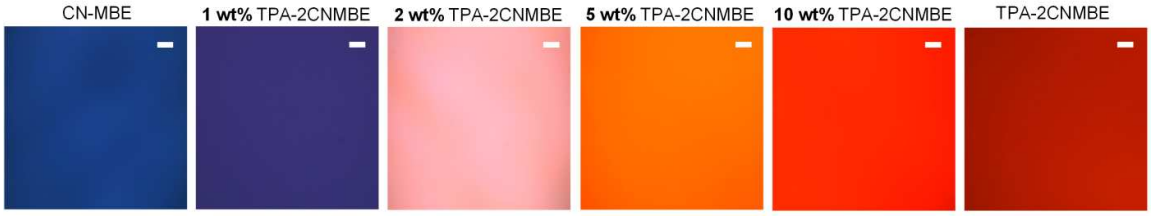

Figure S11. Optical microscopic fluorescence images of CN-MBE/TPA-2CNMBE-doped polymer films with various CN-MBE/TPA-2CNMBE molar ratios; 0, 1, 2, 5, 10, 100 wt.% of TPA-2CNMBE with respect to CN-MBE, respectively (images from left to right). Each length of scale bar in the images is 10 μm.

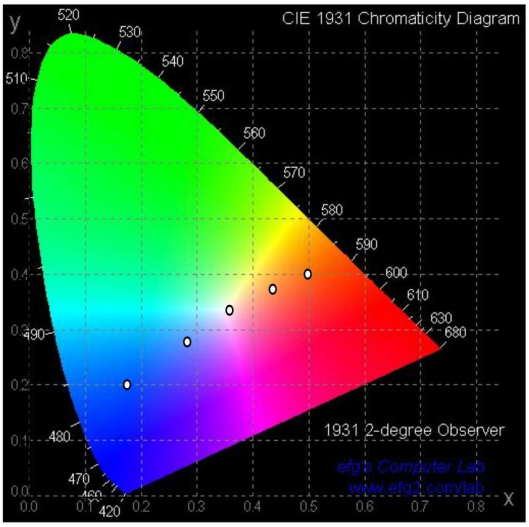

Figure S12. CIE 1931 chromaticity diagram with the fluorescence color of the CN-MBE/TPA-2CNMBE-doped polymer film with various TPA-2CNMBE molar ratios; 0, 1, 2, 5, 10 wt.% of TPA-2CNMBE with respect to CN-MBE, respectively (points from bottom left to up right in the diagram; λ_{ex} = 400 nm).

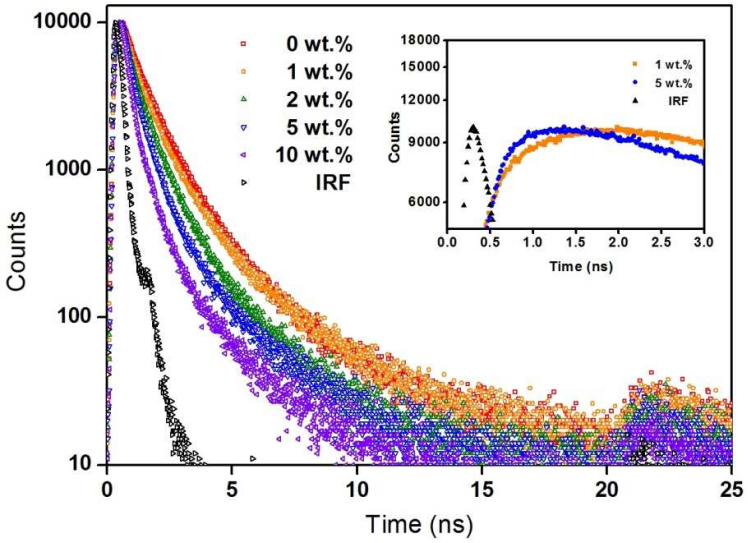

Figure S13. Fluorescence decay profiles of the CN-MBE/TPA-2CNMBE-doped polymer films with various TPA-2CNMBE molar ratios to CN-MBE (λ_{ex} = 377 nm; $\lambda_{monitor}$ = 465 nm in the full profiles, λ_{ex} = 377 nm; $\lambda_{monitor}$ = 653 nm in the inset profiles).

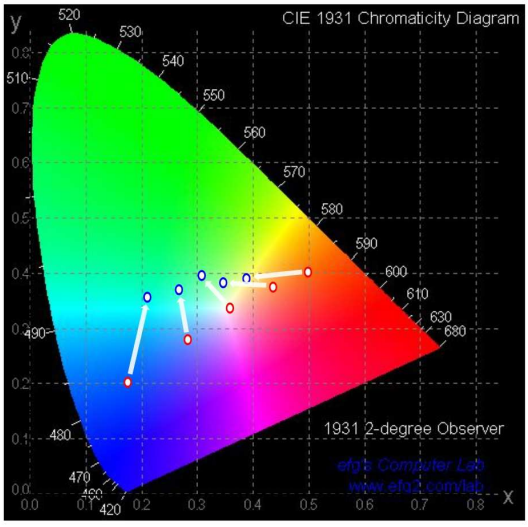

Figure S14. Fluorescence color change via SVA treatment of the CN-MBE/TPA-2CNMBE-doped polymer film with various TPA-2CNMBE molar ratios in a CIE 1931 chromaticity diagram; 0, 1, 2, 5, 10 wt.% of TPA-2CNMBE with respect to CN-MBE, respectively (red points from bottom left to up right in the diagram; λ_{ex} = 400 nm). Blue points exhibit the fluorescence color of the SVA treated films, while red points exhibit that of the films with no treatment.

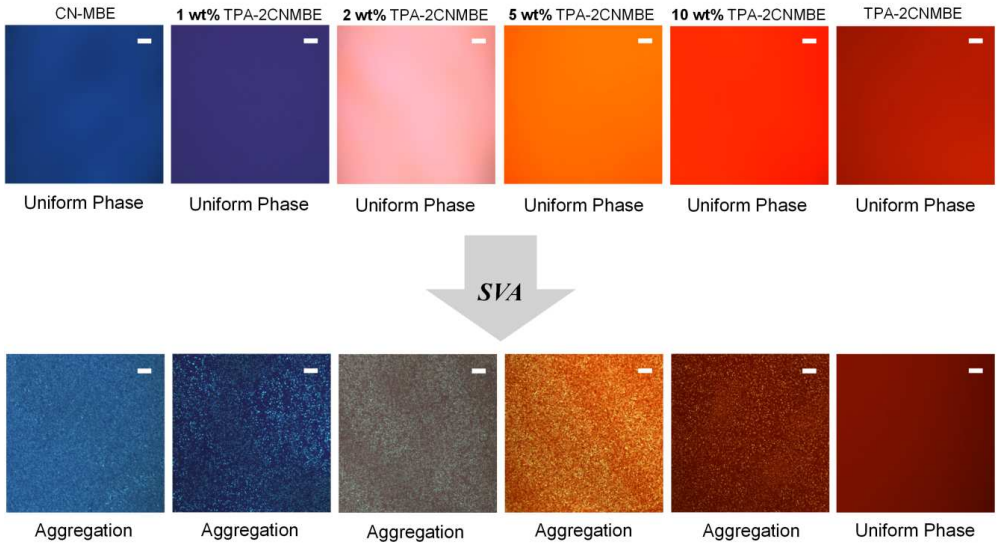

Figure S15. Optical microscopic fluorescence images of CN-MBE/TPA-2CNMBE-doped polymer films with various TPA-2CNMBE molar ratios showing morphology change with aggregation of CN-MBE via SVA treatment (except for only TPA-2CNMBE-doped polymer film); 0, 1, 2, 5, 10, 100 wt.% of TPA-2CNMBE with respect to CN-MBE, respectively (images from left to right). Each length of scale bar in the images is 10 μm.

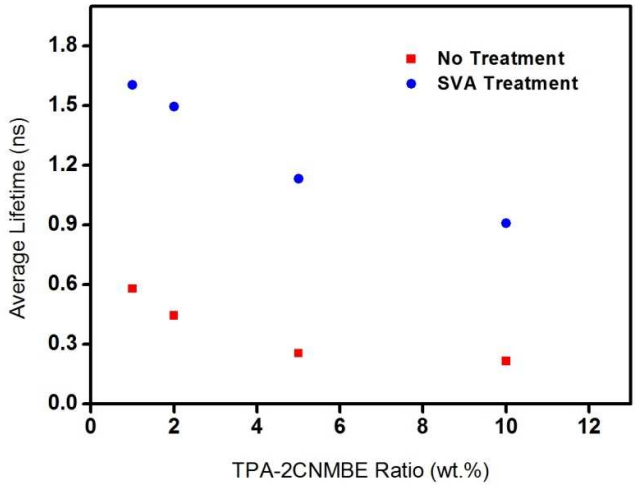

Figure S16. Average lifetime change of CN-MBE/TPA-2CNMBE-doped polymer film with SVA treatment (λ_{ex} = 377 nm; $\lambda_{monitor}$ = 465 nm). Blue points exhibit the values of the SVA treated spin-coated films, while red points exhibit that of the spin-coated films without any treatments.

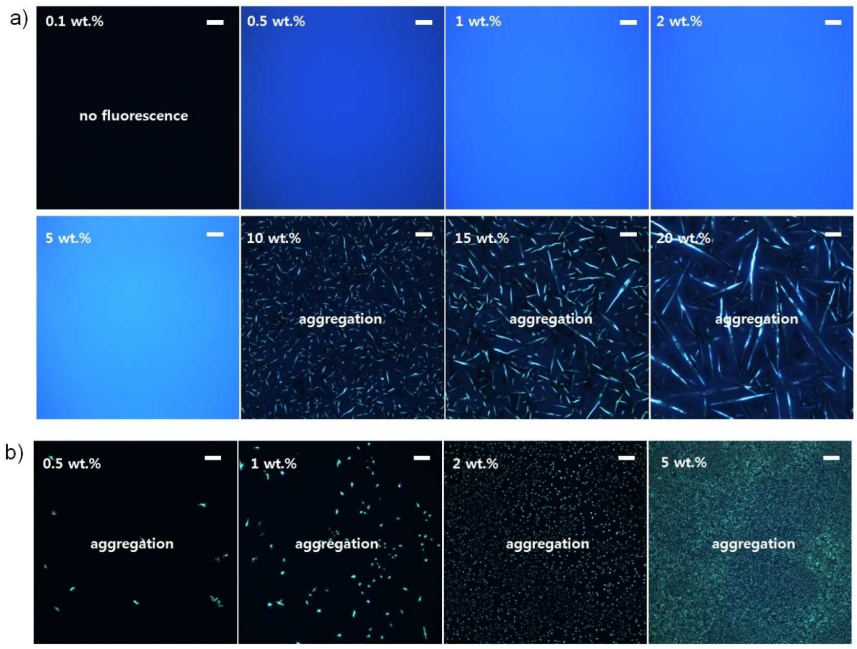

Figure S17. a) Optical microscopic fluorescence images of the CN-MBE-doped polymer films. Concentration of CN-MBE are set to 0.1, 0.5, 1, 2, 5, 10, 15, 20 wt.% with respect to PMMA concentration. It shows occurrence of the aggregation with only spin-coating in the CN-MBE ratio of 10 wt.% and above. b) Optical microscopic fluorescence images of the SVA treated CN-MBE-doped polymer films with various molar ratio of CN-MBE: 0.5, 1, 2, 5 wt.% of CN-MBE with respect to PMMA. It shows occurrence of the aggregation via SVA treatment in all films we tested. Each length of scale bar in the images is 10 μm.

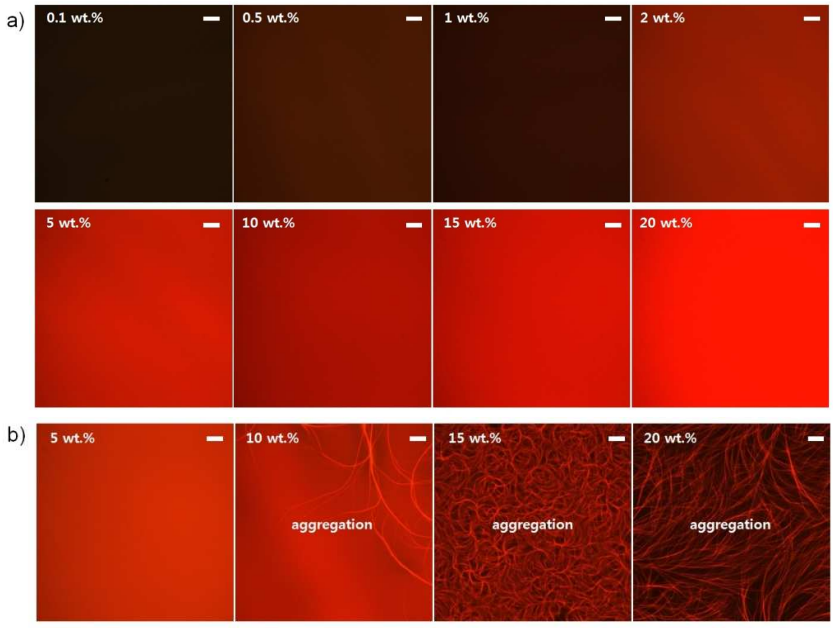

Figure S18. a) Optical microscopic fluorescence images of the TPA-2CNMBE-doped polymer films. Concentration of TPA-2CNMBE are set to 0.1, 0.5, 1, 2, 5, 10, 15, 20 wt.% with respect to PMMA. All spin-coated films are uniform and smooth without any discernible structure. b) Optical microscopic fluorescence images of the SVA treated TPA-2CNMBE-doped polymer films with various molar ratio of TPA-2CNMBE: 5, 10, 15, 20 wt.% of TPA-2CNMBE with respect to PMMA. It shows occurrence of the aggregation via SVA treatment in the TPA-2CNMBE ratio of 10 wt.% and above. Each length of scale bar in the images is 10 μm.

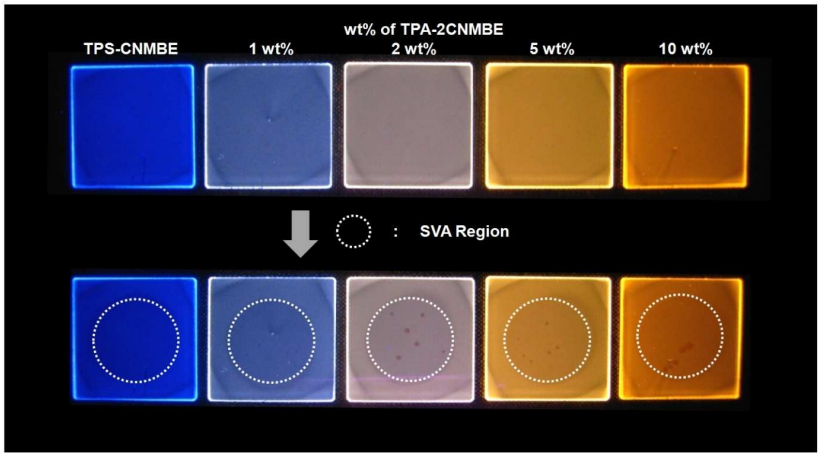

Figure S19. Fluorescence images of TPS-CNMBE/TPA-2CNMBE-doped polymer films with various TPS-CNMBE/TPA-2CNMBE molar ratios; 0, 1, 2, 5, 10 wt.% of TPA-2CNMBE with respect to TPS-CNMBE, respectively (from left to right; λ_{ex} = 365 nm).

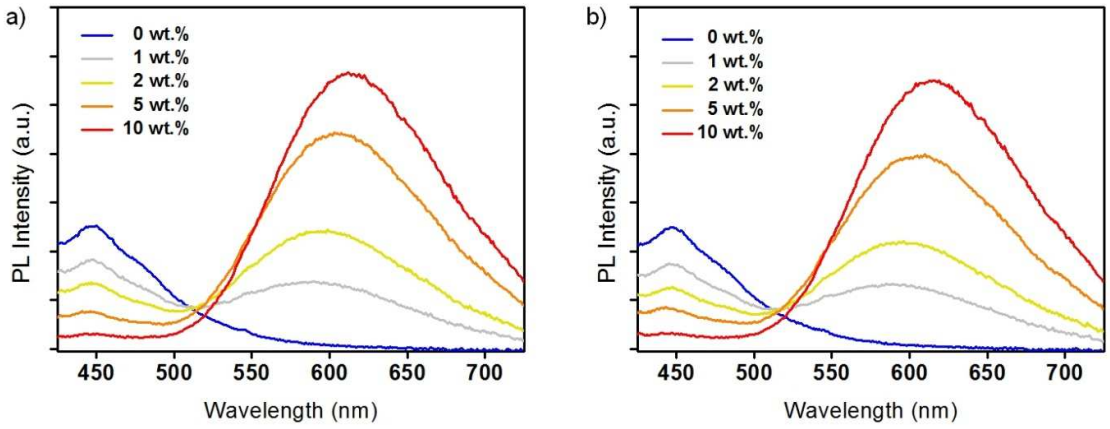

Figure S20. a,b) Fluorescence spectra of the TPS-CNMBE/TPA-2CNMBE-doped polymer films without any treatments (a) and the SVA treated TPS-CNMBE/TPA-2CNMBE-doped polymer films (b) with various TPS-CNMBE/TPA-2CNMBE molar ratios; 0, 1, 2, 5, 10 wt.% of TPA-2CNMBE with respect to TPS-CNMBE, respectively (λ_{ex} = 400 nm).

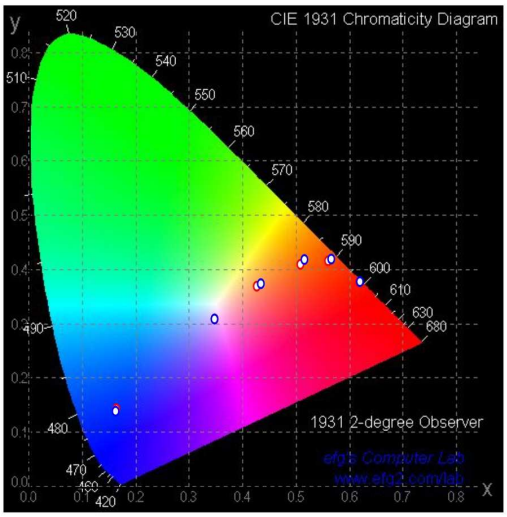

Figure S21. Fluorescence color change via SVA treatment of the TPS-CNMBE/TPA-2CNMBE-doped polymer films with various TPA-2CNMBE molar ratios in a CIE 1931 chromaticity diagram; 0, 1, 2, 5, 10, 100 wt.% of TPA-2CNMBE with respect to TPS-CNMBE, respectively (points from bottom left to up right in the diagram; λ_{ex} = 400 nm). Blue points exhibit the fluorescence color of the SVA treated films, while red points exhibit that of the films with no treatment. Each blue point overlaps with red point of the sample in same ratio.

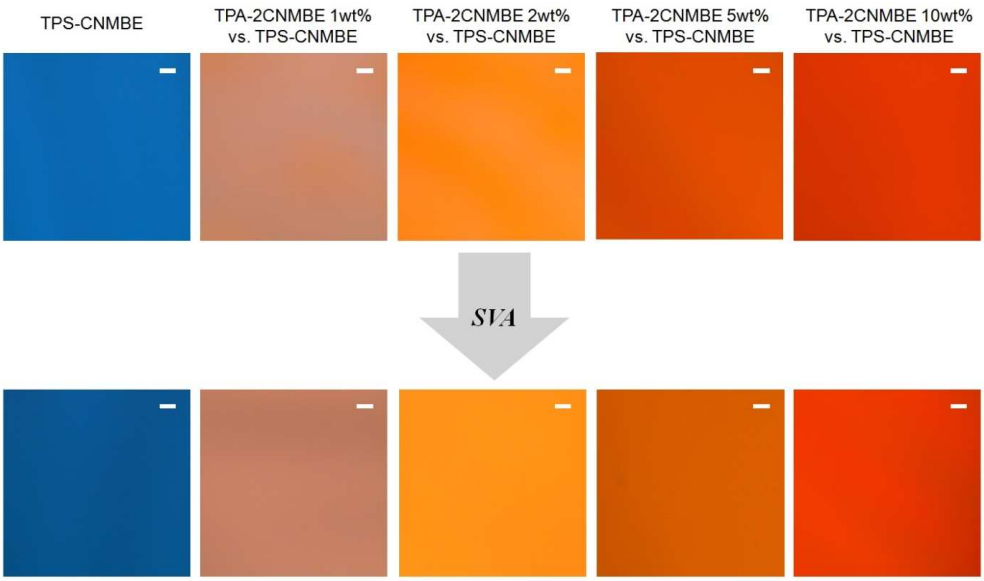

Figure S22. Optical microscopic fluorescence images of the TPS-CNMBE/TPA-2CNMBE-doped polymer films without any treatments (above) and with SVA treatments (below) with various TPS-CNMBE/TPA-2CNMBE molar ratios; 0, 1, 2, 5, 10, wt.% of TPA-2CNMBE with respect to TPS-CNMBE, respectively (images from left to right). Each length of scale bar in the images is 10 μm.

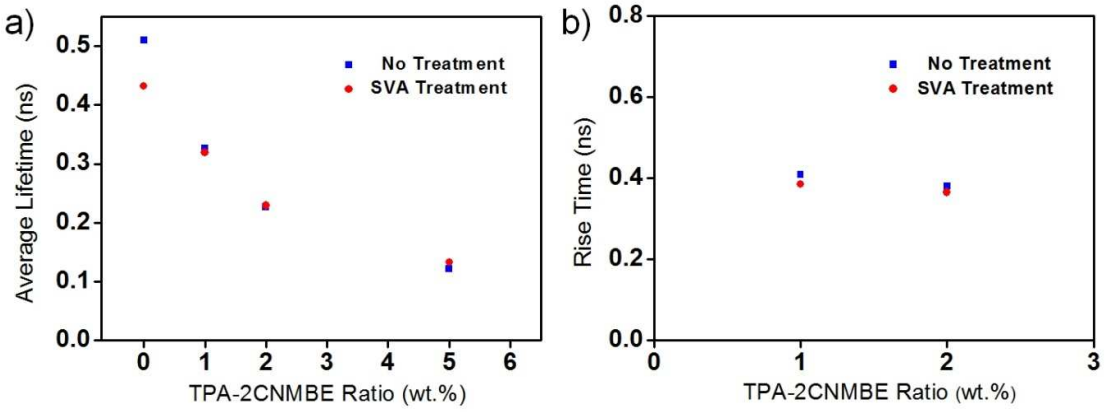

Figure S23. a) Average lifetime of the TPS-CNMBE/TPA-2CNMBE-doped polymer film with various TPA-2CNMBE molar ratios; 0, 1, 2, 5 wt.% of TPA-2CNMBE with respect to TPS-CNMBE, respectively (λ_{ex} = 377 nm; $\lambda_{monitor}$ = 449 nm). b) Rise time the TPS-CNMBE/TPA-2CNMBE-doped polymer film with 1, 2 wt.% of TPA-2CNMBE (λ_{ex} = 377 nm; $\lambda_{monitor}$ = 659 nm).

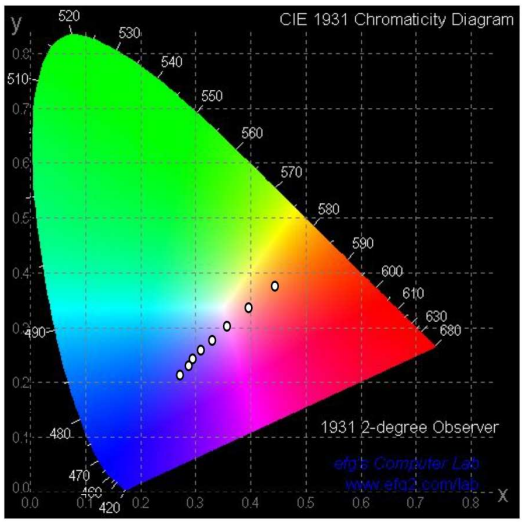

Figure S24. CIE 1931 chromaticity diagram with the fluorescence color (λ_{ex} = 400 nm) of the CN-MBE/TPA-2CNMBE/BP-BTE-doped polymer film with various UV light irradiation time (365 nm); The UV irradiation time was varied 0, 5, 10, 15, 20, 25, 30, 35 seconds, respectively (points from up light to bottom left in the diagram).

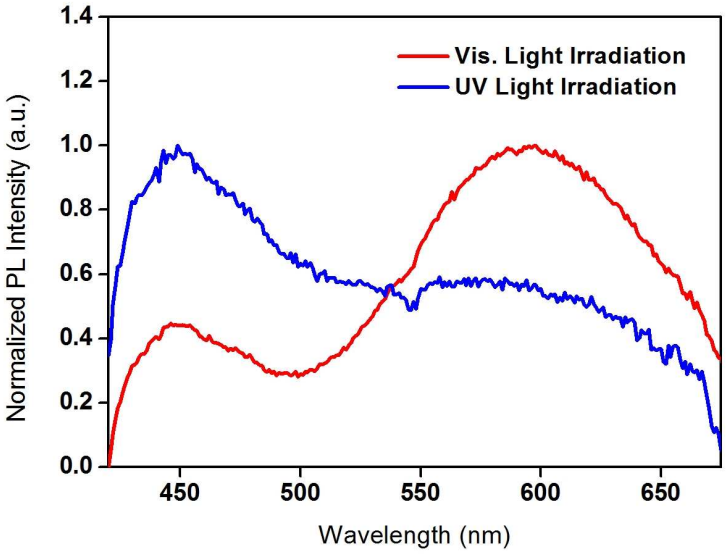

Figure S25. Normalized fluorescence spectra of the CN-MBE/TPA-2CNMBE/BP-BTE-doped polymer film after visible and UV light irradiation (λ_{ex} = 400 nm).

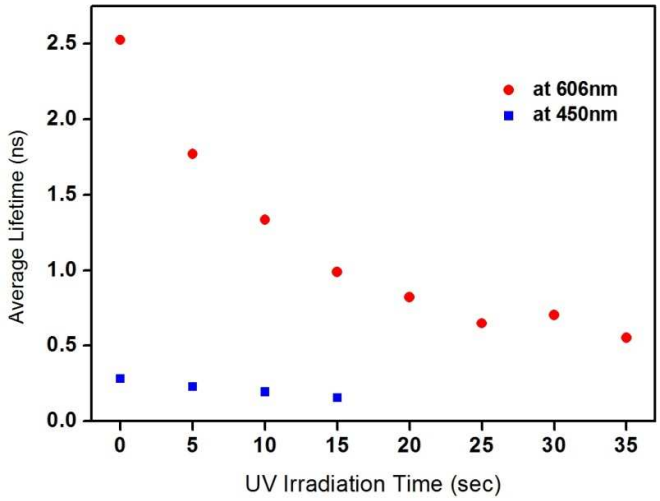

Figure S26. Average lifetime change of the CN-MBE/TPA-2CNMBE/BP-BTE-doped polymer film with UV light (365 nm) irradiation (λ_{ex} = 377 nm; $\lambda_{monitor}$ = 450 nm for blue points, $\lambda_{monitor}$ = 606 nm for red points).

Table S1. Experimental FRET efficiency of the CN-MBE/TPA-2CNMBE-doped polymer films with various TPA-2CNMBE ratios with respect to CN-MBE.

TPA-2CNMBE ratio (wt.%)	1	2	5	10
FRET efficiency (%)	34.5	38.8	63.4	78.8

Table S2. Experimental FRET efficiency of the SVA treated CN-MBE/TPA-2CNMBE-doped polymer films with various TPA-2CNMBE ratios with respect to CN-MBE.

TPA-2CNMBE ratio (wt.%)	1	2	5	10
FRET efficiency (%)	9.9	16.1	22.7	38.2